Observing interference effect in binary (e, 2e) of molecules

Xiangjun Chen[1, 2, *], Jing Yang[1, 2], Xu Shan[1, 2], Zhe Zhang[1], Qiguo Tian[1] and Enliang Wang[1, 2]

[1]Hefei National Laboratory for Physical Sciences at Microscale and Department of Modern Physics, University of Science and Technology of China, Hefei, Anhui, 230026, China
[2]Synergetic Innovation Center of Quantum Information and Quantum Physics, University of Science and Technology of China, Hefei, Anhui 230026, China

E-mail: xjun@ustc.edu.cn

Abstract. We present investigations on the two-center and multi-center interference effects of molecules in binary (e, 2e) experiments. The high energy resolution electron momentum spectroscopy (EMS) measurements on H_2 are reported with final vibrational states resolved. The experimental momentum profiles for ionization transitions to the individual final vibrational states of the ion are obtained. The measured and calculated vibrational ratios of the cross sections deviate from Franck-Condon principle, which can be ascribed to the Young-type two-center interference. Furthermore, with the help of our latest version of EMS spectrometer which has considerably higher sensitivity and much wider momentum range from 0 to 8 a.u., we are able to extend our observations to multi-center interference effect in high symmetry molecules like NF_3 and CF_4 with several oscillation periods included.

1. Introduction

As we all know, particle-wave duality of matter particles plays key role in quantum mechanics. It is one of the prominent conceptual deviations from the classical physics. This revolutionary concept has been directly demonstrated by the beautiful electron double-slit experiment by Clause Jönsson in 1961 [1]. Since then, double-slit experiments have shown the wave character of increasingly larger quantum objects, including fullerenes (buckyballs) [2] and huge organic molecules [3]. Another way to realize the double-slit experiment is the coherent superposition of electrons emitted from two indistinguishable atoms in diatomic molecules [4-22]. This is often referred to as molecular double-slit interference, which was first suggested by Cohen and Fano [4] in 1966 in photoionization of diatomic molecules N_2 and O_2. Such interference effects will lead to the energy- or angle-dependent oscillations in cross sections. It took 35 years before this two-center interference effect was unambiguously proven for H_2 in the ionizations by heavy ions [5], and another 4 more years in 2005 to find evidence in photoionization of N_2 [10].

The interference effect in dipole (e, 2e) ionization of H_2 was first predicted by theoretical calculations in 2003 [17] and then observed by experiments employing coplanar asymmetric kinematics at intermediate energies [18, 19]. The effect was revealed from the suppression or enhancement of the forward (binary) or backward (recoil) scattering peaks as compared to helium at same kinematics. In

* To whom any correspondence should be addressed.

fact, it would be more straightforward to observe Young-type interference in binary (e, 2e). For binary (e, 2e), we have (1) high electron impact energy; (2) larger momentum transfer to ejected electron. If the Bethe ridge condition is satisfied that the incident electron transfers all the lost momentum to target electron, the triple differential cross section (TDCS) of (e, 2e) [23] is then directly linked to the square modulus of the single-electron wave function in momentum space and can be used to directly 'imaging' the electron momentum distributions for individual orbitals. The relevant technique is usually terminized as electron momentum spectroscopy (EMS).

For the simplest diatomic molecule H_2, as a simple approximation, the molecular orbital (MO) ψ can be expressed by a linear combination of atomic orbitals (LCAO):

$$\psi = \frac{1}{\sqrt{2}}(1s_A + 1s_B)\,, \tag{1}$$

where $1s_A$ and $1s_B$ are two identical 1*s* atomic orbitals centered on atoms A and B of the molecule. It is easy to obtain the TDCS [17]

$$\sigma_{EMS}^{(3)} \cong 2[1+\sin(qR_0)/(qR_0)]\sigma_H^{(3)}\,, \tag{2}$$

where $\sigma_H^{(3)}$ is the atomic TDCS, R_0 is the internuclear distance at equilibrium and q is the magnitude of the recoil momentum of residual ion which is equal to p, the magnitude of the momentum of orbital electron, under the EMS condition. In principle, we can directly observe the interference factor $1+\sin(pR_0)/(pR_0)$ by plotting the ratio of TDCSs of molecule and atom as a function of momentum p. Such phenomena is also called bond oscillation [24, 25] and its prediction can be traced back to the early 1940s [26]. However, for H_2, it is difficult to observe such interference effect for two reasons. Firstly, the momentum range for a conventional EMS instrument is limited to 0 ~ 3.0 a.u. A much wider range of momenta up to $2\pi/R_0$ = 4.5 a.u.is at least required to observe a complete period of bond oscillation in H_2, having the internuclear distance R_0 of 1.4 a.u. Secondly, the EMS cross section decreases very rapidly as momentum increases. In order to have clear observations of interference effect, one way is to choose a molecule having larger internuclear distance. Most recently, the multi-centre interference effect was observed in binary (e, 2e) experiment for the three outermost MOs of CF_4 [22], each of which are consisted of a combination of non-bonding 2*p* AOs located on the four F atoms. The F-F internuclear distance is 4.02 a.u. and the period $2\pi/R_0$ = 1.6 a.u. is well located in the momentum range of EMS. Another way to observe the interference effect is to compare the interference factor at different internuclear distance. In this talk, we present our first measurement [27] on vibrationally resolved EMS of H_2 by a high-resolution (e, 2e) spectrometer [28]. The experimental momentum profiles for ionization transitions to the individual final vibrational states of the ion are obtained. By choosing different vibrational states, we equivalently change the internuclear distance. The measured and calculated vibrational ratios of cross sections reveal obvious deviations from Franck-Condon values. Such deviations can be ascribed to the Young-type two-center interference. Furthermore, with the help of our latest version of EMS spectrometers [29] which have considerably higher sensitivity and much wider momentum range from 0 to 8 a.u., we are able to extend our observations to multi-center interference effect in high symmetry molecules like NF_3 and CF_4.

2. Background

EMS is based on the (*e*, 2*e*) experiment in which an electron from target atom or molecule is cleanly knocked out by a high-energy incident electron and the residual ion acts as a spectator. From energy and momentum conservation, the binding energy ε_f and the momentum $\boldsymbol{p}$ of the target electron are given by

$$\varepsilon_f = E_0 - E_a - E_b \tag{3}$$

$$\boldsymbol{p} = \boldsymbol{p}_a + \boldsymbol{p}_b - \boldsymbol{p}_0 \tag{4}$$

where E_i, $\boldsymbol{p}_i$ (i = 0, a, b) are kinetic energies and momenta of the incident and two outgoing electrons, respectively.

Within the binary-encounter approximation, as well as the plane wave impulse approximation (PWIA), the TDCS for (e, 2e) ionization is [23]

$$\frac{d^3\sigma}{d\Omega_a d\Omega_b dE_b} = (2\pi)^4 \frac{p_a p_b}{p_0} f_{ee} \sum_{av} |\langle \boldsymbol{p}I|G\rangle|^2 \tag{5}$$

Here f_{ee} is the electron-electron collision factor which is essentially constant in EMS conditions. Therefore the cross section is proportional to a structure term which is the square of overlap between the initial target state G and final ion state I. $\sum_{av}$ denotes a sum for final states and average for initial states that are not resolved in the experiment and are considered as degenerate. For molecular target the initial state G and final state I can be described in terms of Born-Oppenheimer approximation which is a product of separate electronic, vibrational, and rotational functions [23]:

$$|G\rangle = |0V_\mu D_\nu\rangle \tag{6}$$

$$|I\rangle = |iV'_{\mu'} D'_{\nu'}\rangle \tag{7}$$

where V_μ and D_ν are the vibrational and rotational functions for the initial state. The indices μ and ν represent quantum numbers that specify the vibrational and rotational states respectively. Final vibrational and rotational quantities are denoted by primes. The notations 0 and i represent the electronic states of target and ion. At room temperature the target is in its vibrational ground state V_0 ($\mu = 0$).

For the conventional EMS spectrometer, the energy resolution (typically 1~2 eV) cannot resolve the final vibrational and rotational states. The cross section reduces to

$$\sum_{av} |\langle \boldsymbol{p}I|G\rangle|^2 = \int \frac{d\Omega}{4\pi} \langle V_0 || \langle \boldsymbol{p}i|0\rangle|^2 |V_0\rangle \tag{8}$$

For the H_2 molecule Dey *et al.*[30] showed that the vibrational average gives the same results as taking the electronic functions at their equilibrium nuclear geometry. This approximation has subsequently been justified by agreement with a wide range of experiments. So the cross section further reduces to

$$\sigma^{(3)}_{EMS} = \frac{d^3\sigma}{d\Omega_a d\Omega_b dE_b} \propto \int \frac{d\Omega}{4\pi} |\langle \boldsymbol{p}i|0\rangle|^2 \tag{9}$$

The integral in equation (9) is known as the spherically averaged electron momentum distribution, or electron momentum profile.

3. Two-center interference effects in vibrationally resolved (e, 2e) of H_2

Figure 1(a) illustrates the ionization process involved in this work - vibronic transition from $X^1\Sigma_g^+$ ground state of H_2 to $^2\Sigma_g^+(1s\sigma_g)$ ground state of H_2^+ ion. At room temperature the ionization starts from μ = 0 vibrational ground state of target to a certain μ' vibrational state of ion. Figure 1(b) shows the ionization energy spectrum obtained by high-resolution photoelectron spectroscopy (PES) [31]. The final vibrational states of H_2^+ are well resolved and the relative intensities of the individual vibrational peaks are proportional to the Franck-Condon factors. The binding energy spectrum (BES) measured in this work is shown in figure1(c). Although the energy resolution (0.6 eV) is still not enough to resolve individual vibrational states, the shape of the profile reveals remarkably asymmetric, which is obviously the Franck-Condon profile arising from a series of vibrational excitations.

A least-squares fitting has been carried out utilizing a set of Gaussian functions for individual ionization transitions related to different vibrational states of H_2^+ in the BES. The width of each Gaussian function is fixed at present EMS instrumental energy resolution (0.6 eV) as the natural width of vibrational transition is negligible. The position of each Gaussian function is also referred to the exact energy position of the corresponding vibrational peak determined by high-resolution PES [31]. Thirteen Gaussian functions are used to identify the transitions related to the first thirteen vibrational states with vibrational quantum number $\mu' = 0 \sim 12$, respectively, and another one more function to fit the states with $\mu' > 12$. The experimental momentum profiles (XMPs), which are the momentum dependent EMS cross sections, can be extracted for individual vibrational states by plotting areas under the

corresponding fitted peaks as a function of target electron momentum. The results are shown in figure 2(b)-(k). For μ'> 8 only the summation is plotted in figure 2(k) due to the large uncertainty of data. As can be seen from the figures, all the XMPs show the typical *s*-type character due to the ionization from $1s\sigma_g$ of H_2. Also included in the figures for comparison are the theoretical momentum profiles (TMPs) calculated by

$$\frac{d^3\sigma}{d\Omega_a d\Omega_b dE_b} \propto \int \frac{d\Omega}{4\pi} \left| \langle \boldsymbol{p} V'_{\mu'} i | 0 V_0 \rangle \right|^2 \tag{10}$$

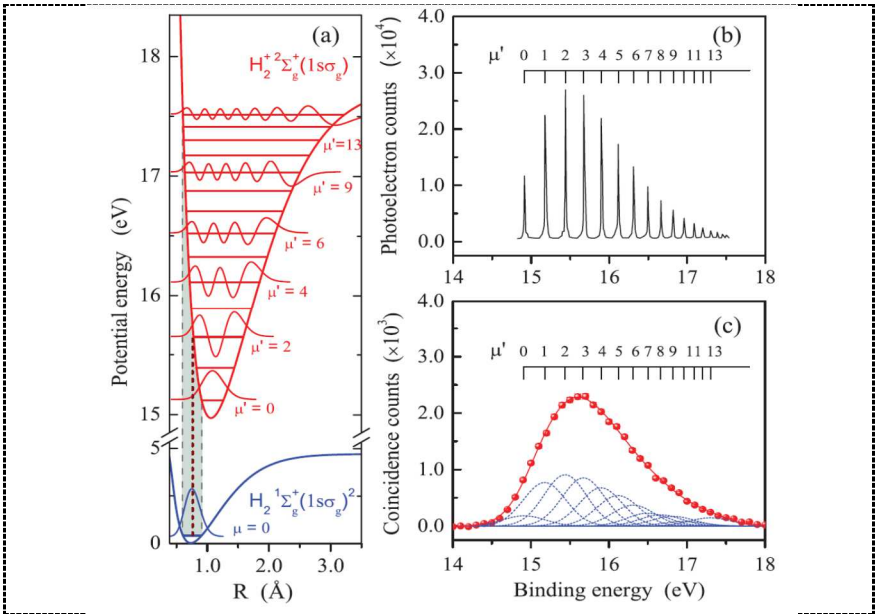

Figure 1. (a) The vibronic transitions from $X\,{}^1\Sigma_g^+$ ground state of H_2 to ${}^2\Sigma_g^+(1s\sigma_g)$ ground state of H_2^+. The wave functions of some vibrational states are also showed. (b) The high-resolution photoelectron spectrum of H_2. (c) The BES of H_2 obtained in present experiment. The dash lines indicate the Gaussian peaks, and the solid line is the summed fit.

For H_2 molecule which has only one vibrational mode, the structure amplitude $\langle \boldsymbol{p} V'_{\mu'} i | 0 V_0 \rangle$ can be simplified as

$$\langle \boldsymbol{p} V'_{\mu'} i | 0 V_0 \rangle = \int dR \mathrm{X}^*_{\mu'}(R) \mathrm{X}_0(R) S^{(i)}(R) \varphi(\boldsymbol{p}, R) \tag{11}$$

where $S^{(i)}(R) = \int d\boldsymbol{\tau} \phi_i(\boldsymbol{\tau}, R) \psi(\boldsymbol{\tau}, R)$ is the overlap integral of the wave functions for the final ion and molecular residue left after the knockout of an electron from molecular orbital, and $\varphi(\boldsymbol{p}, R) = (1/2\pi)^{3/2} \int d\boldsymbol{r} e^{-i\boldsymbol{r}\cdot\boldsymbol{p}} \psi(\boldsymbol{r}, R)$ is the Fourier transform of $\psi(\boldsymbol{r}, R)$. $\mathrm{X}_0(R)$ and $\mathrm{X}_{\mu'}(R)$ are vibrational wave functions of H_2 and H_2^+. The TMPs are convoluted with instrumental momentum resolution of 0.10 a.u. and all the TMPs and XMPs in the figures are area-normalized to unity. The agreements in shape between experiments and theoretical calculations are fairly good. Although the experimental uncertainties are rather large, the general trend that XMP becomes 'fatter' with increase of vibrational quantum number is somehow observable.

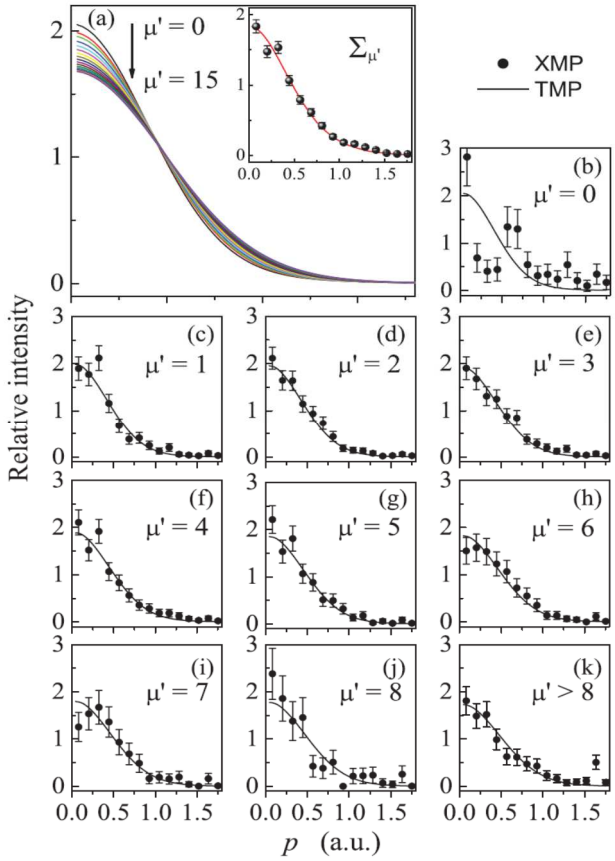

Figure 2. (a) The TMPs for different H_2^+ vibrational states (shown by different colors). The inset shows the summed XMP for all final vibrational states compared with the TMP calculated at equilibrium nuclear distance. The XMPs and corresponding TMPs for μ′ =0~8 are shown in (b)-(j), respectively. The XMP and TMP presented in (k) are the sum of XMPs and TMPs for μ′ >8. All profiles in this figure are area-normalized.

To highlight the differences, vibrational ratios of EMS cross sections are plotted in figure 3. We group the final vibrational states into three: the low quantum number group with $\mu' = 0,1,2$ denoted by capital letter *L*, the intermediate quantum number group with $\mu' = 4,5,6$ denoted by *I* and the high quantum number group with $\mu' = 9 \sim 13$ denoted by *H*. The theoretical EMS cross section $\sigma_{EMS}(15)$ for $\mu' = 15$ is chosen as a reference, and the summed EMS cross sections of both experiments and theoretical calculations for these three groups are all divided by the reference $\sigma_{EMS}(15)$. The 'experimental' and theoretical results of $\sigma_{EMS}(X)/\sigma_{EMS}(15)$ ($X = L, I, H$) are shown in figure 3(a)-(c) by solid circles and curves respectively. Here, $\sigma_{EMS}(X)$ are again area-normalized to unity respectively for the convenience of comparison. Using Franck-Condon (FC) approximation, equation (11) is reduced to

$$\langle \boldsymbol{p} V'_{\mu'} i | 0 V_0 \rangle = g_0^{\mu'} S^{(i)}(R_0) \varphi(\boldsymbol{p}, R_0) \tag{12}$$

where $g_0^{\mu'} = \int dR \mathrm{X}_{\mu'}(R) \mathrm{X}_0(R)$ is the FC factor. Within this approximation, the ratio of EMS cross sections for two final vibrational states $\sigma_{EMS}(\mu_1')/\sigma_{EMS}(\mu_2')$ will be equal to the quotient of the relevant FC factor $g_0^{\mu_1'}/g_0^{\mu_2'}$, which will keep as a constant in the whole momentum range. However, one can

see immediately from figure 3(a)-(c) that the observed ratios of $\sigma_{EMS}(X)/\sigma_{EMS}(15)$ ($X = L, I, H$) obviously deviates from constant (here is unity due to the normalization), especially the low quantum number group '*L*' whose ratio declines sharply with the momentum. The deviation from the FC principle can be ascribed to the two-center interference effect. When taking into account vibrational states, the vibrationally resolved cross section can be approximated by

$$\sigma_{EMS}(\mu') = \sigma_0 \left| \int_0^\infty \mathrm{X}_{\mu'}(R) \left[1 + \frac{\sin(pR)}{pR} \right]^{1/2} \mathrm{X}_0(R) dR \right|^2 \tag{13}$$

where σ_0 is the equivalent one center atomic cross section. By replacing in equation (13) the variable *R* by characteristic value $R_{\mu'}$ associated with μ'state, the vibrational ratio can further be approximated by

$$\frac{\sigma_{EMS}(\mu_1')}{\sigma_{EMS}(\mu_2')} = \frac{g_0^{\mu_1'}}{g_0^{\mu_2'}} \left[1 + \frac{\delta R_{\mu_1'}}{R_{\mu_2'}} \cos(pR_{\mu_2'}) \right] \tag{14}$$

This formula clearly predicts that the vibrational ratio should oscillate around the quotient of FC factor. To evaluate the observations, the turning points on potential curve for relevant vibrational states are adopted as the characteristic value $R_{\mu'}$ and the function $a_0 \left[1 + a_1 \frac{\delta R_{\mu_1'}}{R_{\mu_2'}} \cos(pR_{\mu_2'}) \right]$ is employed to fit the vibrational ratios, where a_0 and a_1 are adjustable parameters. The turning point for $\mu_2' = 15$ state is 1.12 a.u., while the averaged values of turning points 1.6 a.u., 1.35 a.u. and 1.15 a.u. are used for $X = L, I, H$ respectively. The parameter a_1 is introduced to compensate the approximations in the evaluations of $R_{\mu'}$ and thus is kept the same value for all three fittings. The fitted curves are presented in figure 3(a)-(c) as chain lines. The agreement of the model fitting with the measured and calculated vibrational ratios undoubtedly signifies the Young's two-center interference effect and the movement of the interference fringe has also been observed. Vibrationally resolved experiment provides a more straightforward way to observe Young-type interference in electron impact ionization of diatomic molecules, which does not rely on the comparison with one-center atomic cross section.

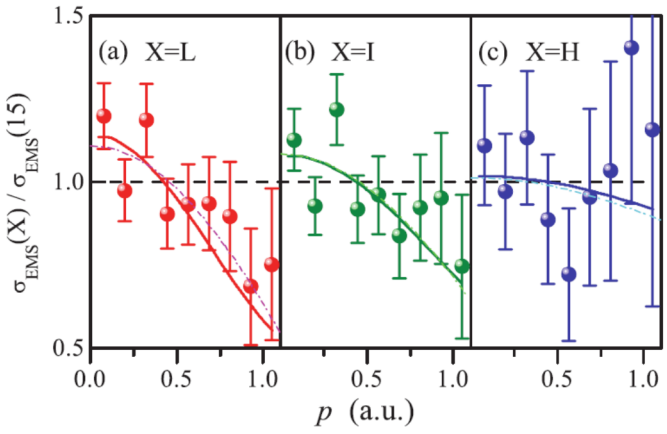

Figure 3. The experimental and theoretical ratios of the EMS cross sections for different groups of vibrational states over the calculated cross section for μ'=15 : (a) the low quantum number group $X = L$; (b) the intermediate quantum number group $X = I$; (c) the high quantum number group $X = H$. Solid circles and curves represent experimental and theoretical results. Dashed lines are Franck-Condon predictions. Chained lines are fitted curves of the model.

4. Multi-center interference effects in (e, 2e) of CF_4 and NF_3

As we have mentioned above, in order to have clear observations of interference effect, one way is to choose a molecule having larger internuclear distance. The multi-centre interference effect was observed in binary (e, 2e) experiment for the three outermost MOs of CF_4 [22] recently. The large F-F internuclear distance makes a complete period of oscillation to be observable. Most recently, a high-sensitivity angle and energy dispersive multichannel electron momentum spectrometer with simultaneous detection in 2π angle range has been developed [29]. The sensitivity of EMS has been improved by employing a double half wedge and strip anode (DH-WSA) position-sensitive detector (PSD) combined with a 90° sector, 2π spherical electrostatic analyzer. Furthermore, much wider momentum range from 0 to 8 a.u. has been achieved, which makes it possible to include more than two periods of oscillation in observations of multi-center interference effect in high symmetry molecules like NF_3 and CF_4. Here, only the results of CF_4 are presented.

In the simple MO theory, the ground state electronic configuration of CF_4 can be written as:

$$(\text{core})^{10}\ \underbrace{(3a_1)^2\,(2t_2)^6}_{\text{inner valence}}\ \underbrace{(4a_1)^2\,(3t_2)^6\,(1e)^4\,(4t_2)^6\,(1t_1)^6}_{\text{outer valence}}\ .$$

The three outermost orbitals are non-bonding, essentially due to the 2*p* lone-pair electrons on fluorine atoms. For these MOs consisting of the F 2p AOs, the TDCS can be expressed as [22]

$$\sigma_{\text{EMS}}(p) \propto \sigma_{2p}(p)\left[1 + C_0\, j_0(pR_{\text{FF}}) + C_2\, j_2(pR_{\text{FF}})\right] \tag{15}$$

where R_{FF} is the internuclear distance between the F atoms and C_0 and C_2 are coefficients of the spherical Bessel functions of order 0 and 2 respectively. The EMS cross section $\sigma_{2p}(p)$ for the 2*p* AO of an isolated F atom is calculated by distorted wave Born approximation employing B3LYP/aug-cc-pVTZ wavefunction. The function $[1 + C_0 j_0(pR_{\text{FF}}) + C_2 j_2(pR_{\text{FF}})]$ governs the oscillatory structure and hence it is the interference factor in this case

$$\sigma_{\text{EMS}}(p)/\sigma_{2p}(p) \propto 1 + C_0\, j_0(pR_{\text{FF}}) + C_2\, j_2(pR_{\text{FF}}). \tag{16}$$

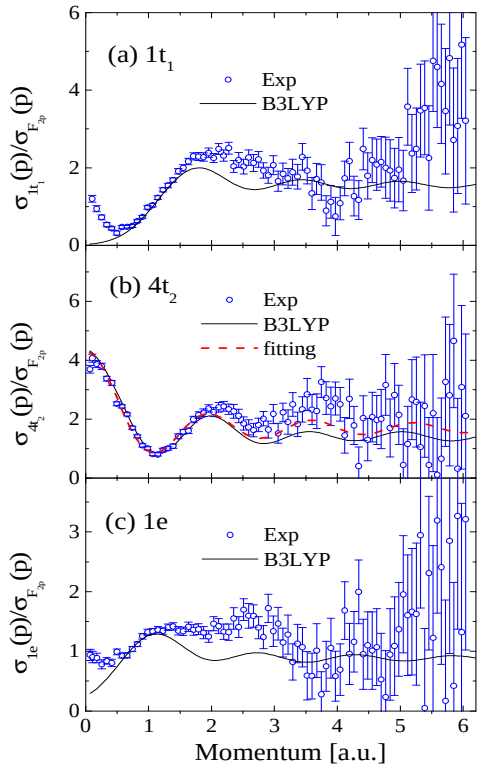

Figure 4. Comparison of experimental and DWBA/B3LYP calculated interference factor for the (a) $1t_1$, (b) $4t_2$, and (c) $1e$ molecular orbitals of CF_4.

The interference factors for the three outermost orbitals of CF_4 are shown in figure 4. It is immediately clear that the experiments exhibit oscillatory structures. Compared to the previous experiment [22], more periods of oscillations are included, further confirming the interference effect. To highlight it more closely, the function $h[1 + C_0 j_0(pR_{FF}) + C_2 j_2(pR_{FF})]$ is subsequently employed as a fitting curve for $4t_2$ to reproduce the experiment with R_{FF}, h, C_0, and C_2 being fitting parameters. The best fit to the experiment is presented also in figure 4(b) by the dashed line. The resulting R_{FF} value is 3.9 Bohr which is in excellent agreement with 4.07 Bohr reported by electron diffraction [32].

Acknowledgments
This work was jointly supported by the National Natural Science Foundation of China (Grant Nos. 11327404, 10734040), the National Basic Research Program of China (Grant No. 2010CB923301).

References

[1] Jönsson C 1961 *Z. Phys.* **161** 454
[2] Arndt M, Nairz O, Vos-Andreae J, Keller C, van der Zouw G and Zeilinger A 1999 *Nature* **401** 680
[3] Gerlich S, Eibenberger S, Tomandl M, Nimmrichter S, Hornberger K, Fagan P J, Tüxen J, Mayor M and Arndt M 2011 *Nature Comunications* **2** 263
[4] Cohen D and Fano U 1966 *Phys. Rev.* **150** 30
[5] Stolterfoht N *et al.* 2001 *Phys. Rev. Lett.* **87** 23201
[6] Misra D, Kadhane U, Singh Y P *et al.* 2004 *Phys. Rev. Lett.* **92** 153201
[7] Schmidt H T, Fischer D, Berenyi Z *et al.* 2008 *Phys. Rev. Lett.* **101** 083201
[8] Misra D, Schmidt H T, Gudmundsson M *et al.* 2009 *Phys. Rev. Lett.* **102** 153201
[9] Voitkiv A B, Najjari B and Fischer D 2011 *Phys. Rev. Lett.* **106** 233202
[10] Rolles D, Braune M, Cvejanović S *et al.* 2005 *Nature* **437** 711
[11] Fernández J, Fojón O, Palacios A and Martín F 2007 *Phys. Rev. Lett.* **98** 043005
[12] Akoury D, Kreidi K, Jahnke T *et al.* 2007 *Science* **318** 949
[13] Kreidi K, Akoury D, Jahnke T *et al.* 2008 *Phys. Rev. Lett.* **100** 133005
[14] Zimmermann B, Rolles D, Langer B *et al.* 2008 *Nature Physics* **4** 649
[15] Canton S E, Plésiat E, Bozek J D *et al.* 2011 *PNAS* **108** 7302
[16] Kushawaha R K, Patanen M, Guillemin R *et al.* 2013 *PNAS* **110** 15201
[17] Stia C R, Fojón O A, Weck P F *et al.* 2003 *J. Phys. B* **36** L257
[18] Milne-Brownlie D S, Foster M, Gao J *et al.* 2006 *Phys. Rev. Lett.* **96** 233201
[19] Staicu-Casagrande E M *et al.* 2008 *J. Phys. B* **41** 025204
[20] Kamalou O, Chesnel J Y, Martina D *et al.* 2005 *Phys. Rev. A* **71** 010702(R)
[21] Ozer Z N, Chaluvadi H, Ulu M *et al.* 2013 *Phys. Rev. A* **87** 042704
[22] Watanabe N, Chen X J and Takahashi M 2012 *Phys. Rev. Lett.* **108** 173201
[23] McCarthy I E and Weigold E 1991 *Rep. Prog. Phys.* **54** 789.
[24] Epstein I R and Tanner A C, in *Compton Scattering*, edited by B. G. Williams (McGraw-Hill, New York, 1977)
[25] Cook J P D and Brion C E 1982 *Chem. Phys.* **69** 339
[26] Coulson C A 1941 *Proc. Cambridge Philos. Soc.* **37** 55;
Coulson C A and Duncanson W E 1941 *Proc. Cambridge Philos. Soc.* **37** 67
[27] Zhang Z, Shan X, Wang T *et al.* 2014 *Phys. Rev. Lett.***112** 023204
[28] Shan X, Chen X J, Zhou L X *et al.* 2006 J. Chem. Phys. **125**, 154307 (2006)
[29] Tian Q G, Wang K D, Shan X and Chen X J 2011 *Rev. Sci. Instrum.* **82** 033110
[30] Dey S, McCarthy I E, Teubner P and Weigold E 1975 *Phys. Rev. Lett.* **34** 782
[31] Pollard J E 1982 *J. Chem. Phys.* **77** 34
[32] Fink M, Schmiedekamp C W and Gregory D 1979 *J. Chem. Phys.* **71** 5238